Improvements in September Arctic sea ice predictions via assimilation of summer CryoSat-2 sea ice thickness observations

Yong-Fei Zhang[1], Mitchell Bushuk[2], Michael Winton[2], Bill Hurlin[2], William Gregory[1], Jack Landy[3], Liwei Jia[2,4]

[1]Atmospheric and Oceanic Sciences Program, Princeton University, Princeton, New Jersey
[2]National Oceanic and Atmospheric Administration/Geophysical Fluid Dynamics Laboratory, Princeton, New Jersey
[3]Centre for Integrated Remote Sensing and Forecasting for Arctic Operations, Department of Physics and Technology, UiT The Arctic University of Norway, Tromsø, Norway
[4]University Corporation for Atmospheric Research, Boulder, Colorado

Key Points:

- The representation of Arctic sea ice volume anomalies is significantly improved by assimilating year-round SIT observations from CryoSat-2.
- Arctic summer sea ice prediction skill is generally improved when initial conditions are constrained by satellite SIT observations.
- The Arctic summer sea ice in the 2010s decade is particularly hard to predict due to anomalously low correlation between volume and extent.

Corresponding author: Yong-Fei Zhang, yongfeiz@princeton.edu

Abstract

Because of a spring predictability barrier, the seasonal forecast skill of Arctic summer sea ice is limited by the availability of melt-season sea ice thickness (SIT) observations. The first year-round SIT observations, retrieved from CryoSat-2 from 2011–2020, are assimilated into the GFDL ocean–sea ice model. The model's SIT anomaly field is brought into significantly better agreement with the observations, particularly in the Central Arctic. Although the short observational period makes forecast assessment challenging, we find that the addition of May–August SIT assimilation improves September local sea ice concentration (SIC) and extent forecasts similarly to the early addition of SIC assimilation. Although most regional forecasts are improved by SIT assimilation, the Chukchi Sea forecasts are degraded. This degradation is likely due to the introduction of negative correlations between September SIC and earlier SIT introduced by SIT assimilation, contrary to the increased correlations found in other regions.

Plain Language Summary

The dramatic decline of Arctic sea ice, especially in summer, has received a lot of attention. The ability to better predict Arctic summer sea ice several months ahead of time will help decision making on protecting local communities and ecosystems and regulating economic activities in the Arctic. Climate dynamical models have shown reasonable skill in predicting Arctic summer sea ice on seasonal timescales, but also contain considerable errors. Integrating observed sea ice thickness conditions into the model in the summer melt season has a large potential to reduce such errors. This study combines a new year-round satellite sea ice thickness observational product with the sea ice and ocean dynamical model at GFDL and examines its impact on the seasonal prediction of Arctic sea ice. We find that the prediction skill has been improved in general, although some uncertainties exist due to the limited temporal availability of the observations.

1 Introduction

As a key climate change indicator, Arctic sea ice has been declining rapidly in the past few decades, especially in summer (Stroeve & Notz, 2018). This raises concerns as it has broad impacts on both local and global climate, ecosystems, and human society (Meier et al., 2014). Arctic sea ice loss brings challenges to local communities whose lifestyle heavily relies on sea ice and also attracts new economic activity (e.g., oil extraction, mining, and shipping). Subseasonal-to-seasonal predictions of Arctic summer sea ice have therefore become critical for stakeholder planning and decision making. Studies have shown that the current climate forecast systems are able to produce skillful predictions of pan-Arctic sea ice extent (SIE) (Merryfield et al., 2013; Chevallier et al., 2013; Sigmond et al., 2013; Peterson et al., 2015) and regional SIE (Sigmond et al., 2016; Bushuk et al., 2017; Dirkson et al., 2019). The actual prediction skill, however, is considerably lower than the models' potential predictability, which is partially due to the lack of knowledge of sea ice initial conditions (Bushuk et al., 2019).

The anomaly persistence and re-emergence of sea ice concentration (SIC), volume (SIV), and upper ocean heat content are the major predictability sources of Arctic sea ice (Blanchard-Wrigglesworth et al., 2011). While sea surface temperature (SST) has been commonly assimilated into operational systems and proven to improve sea ice predictions (Bushuk et al., 2019; Kimmritz et al., 2019; Dai et al., 2020), the direct assimilation of sea ice observations is at its early stage. The most commonly assimilated observation is satellite SIC because of its good spatial and temporal coverage. The assimilation of SIC has been shown to improve the modeled SIC significantly in different model systems (Lisæter et al., 2003; Lindsay & Zhang, 2006; Tietsche et al., 2013; Kimmritz et al., 2018; Zhang et al., 2018, 2021). The benefits of SIC DA on predictions of Arctic sea ice have been studied at sub-seasonal (Van Woert et al., 2004; Caya et al., 2010) and

seasonal (Massonnet et al., 2015; Kimmritz et al., 2019) time scales. Zhang et al. (2022) conducted a comprehensive evaluation of SIC DA and showed that the subseasonal-to-seasonal predictions of Arctic summer sea ice are improved at both regional and grid-cell levels.

Compared to SIC, SIT satellite observations have more limited temporal coverage. Early SIT retrievals from IceSat-1 campaigns provided coverage in October-November and February-March over 2003–2008 (Kwok & Cunningham, 2008), whereas the more recent Soil Moisture and Ocean Salinity (SMOS; Tian-Kunze et al. (2014)) and CryoSat-2 (Laxon et al., 2013) satellites provide continuous winter SIT data from 2010–present, and the IceSat-2 satellite provides winter data from 2018–present (Petty et al., 2020). Several studies have shown that assimilating these winter satellite-retrieved SIT observations leads to improvements in the simulation of both SIC and SIT (Yang et al., 2014; Xie et al., 2016; Chen et al., 2017; Mu et al., 2018; Fritzner et al., 2019). Blockley and Peterson (2018) was the first study to demonstrate that by assimilating winter satellite SIT observations, the September Arctic SIE predicted from May 1st intialized reforecast experiments could be significantly improved compared to an experiment with no SIT assimilation. However, their improvement is mostly from the reduced model bias and did not assess the benefits of the observed SIT anomalies. Due to the shortness of the data record, no studies have explored the potential benefits of SIT DA on improving predictions of SIE interannual variability.

Dynamical and statistical prediction systems have been found to consistently display an Arctic sea ice spring predictability barrier, in which forecasts initialized before June 1 have much lower skill than the forecasts initialized after (Bonan et al., 2019; Bushuk et al., 2020; Zeng et al., 2023). Therefore, the conventional satellite-retrieved winter SIT observations are likely sub-optimal for improving summer Arctic sea ice predictions. Landy et al. (2022) derived the first year-round Arctic SIT observations spanning 2011–2020 and showed a notable positive correlation between the observed pan-Arctic SIV in the melting season and summer SIE, which shows bright prospects for improving summer Arctic sea ice predictions.

Motivated by these potential prediction improvements, we have developed a sea ice data assimilation framework with the GFDL sea ice–ocean model (MOM6/SIS2) and the Data Assimilation Research Testbed (DART). This study presents a methodology for joint assimilation of SIT and SIC in a multi-category sea ice modeL, and explore the additional benefit of SIT DA in Arctic sea ice summer predictions relative to a system that only assimilates SIC. We describe the data assimilation system and techniques in Section 2, present results in Section 3, and Discussion and Conclusions in Section 4.

2 Materials and Methods

2.1 The GFDL SPEAR Prediction System

The Seamless System for Prediction and EArth System (SPEAR), the current seasonal to decadal prediction system at GFDL, is used in this study. SPEAR uses the latest version of the GFDL atmosphere, land, ocean and sea ice models (Delworth et al., 2020). The spatial resolution for ocean and sea ice models is 1 degree and has two options for atmosphere and land: 1 degree (SPEAR_LO) and 0.5 degree (SPEAR_MED). SPEAR_LO and SPEAR_MED have similar skill in predicting regional Arctic sea ice (Bushuk et al., 2022), so we use SPEAR_LO in this study considering the computational cost.

2.2 Assimilated Observations

We assimilate daily SIC retrievals from the Scanning Multichannel Microwave Radiometer (SMMR) on the Nimbus-7 satellite and the Special Sensor Microwave/Imager

(SSM/I) sensors on the Defense Meteorological Satellite Program's (DMSP) satellites, processed by the National Snow and Ice Data Center (NSIDC) using the NASA Team algorithm (Cavalieri et al., 1996).

We also assimilate year-round SIT observations retrieved from CryoSat-2 satellite measurements from Landy et al. (2022). They use a deep learning technique to discriminate melt ponds from open leads (Dawson et al., 2022), and retrieve freeboard from the radar altimetry observations of sea ice. The freeboard is then corrected for an electromagnetic range bias in the CryoSat-2 radar data and converted to SIT using snow depth data from the Lagrangian Snow Evolution Model (Liston et al., 2020). The original data is biweekly and has a spatial resolution of 80 km. We regrid the data to the SPEAR nominal 1° sea ice and ocean resolution and perform piecewise interpolation to get daily data. For any given month, the first/second observation of a month is assigned to the first/second half of the month. For example, to generate the initial condition for the June 1st forecast, the DA process stops at May 31st, in which no future data is used. The SIT anomalies (SITA) for each day are obtained by removing the 10-year climatology from 2011 to 2020. They are then added to the climatology from the SIC DA historical run to get the SIT data to be assimilated. The reason for assimilating SITA instead of SIT is stated in the next section.

2.3 Data Assimilation Framework and Experiments

Two data assimilation experiments using the GFDL MOM6/SIS2 model configured as in SPEAR_LO and forced by the JRA55do atmospheric reanalysis (Tsujino et al., 2018) are conducted to generate initial conditions: SICDA_IC assimilates SIC observations only and SITDA_IC assimilates both SIC and SITA observations. Observations are assimilated every 5 days from 2011 to 2020. The DA frequency of every 5 days is chosen to match our earlier SIC DA study (Zhang et al., 2021), which considers the computational cost. The baseline experiment SSTrest_IC does not assimilate any sea ice observations but otherwise shares the same configuration with the DA experiments. In all the initialization experiments, SST is nudged towards daily Optimum Interpolation Sea Surface Temperature (OISST; Reynolds et al. (2007)) where observed SIC is lower than 30% (Lu et al., 2020).

The Ensemble Adjustment Kalman Filter (EAKF; Anderson (2001)) is applied to assimilate observations. We perturb sea ice model parameters to generate 30 ensemble members of MOM6/SIS2. In addition to the ice strength and albedo parameters that are perturbed in Zhang et al. (2021), the snow conductivity parameter is also perturbed, which increases the ensemble spread of SIT and was found to improve assimilation performance. The ice strength parameter P^* from Hibler (1979) follows a uniform distribution between 20000 and 50000 Nm^{-2} (the default value is 27500 Nm^{-2}). The albedo parameters of snow R_{snw}, ice R_{ice}, and pond R_{pnd} from (Briegleb & Light, 2007) follow a random uniform distribution between -1.6 and 1.6 standard deviations (the default value is 0). The snow conductivity follows a uniform distribution between 0.2 and 0.5 $\mathrm{Wm}^{-1}\mathrm{K}^{-1}$ (default value is 0.31 $\mathrm{Wm}^{-1}\mathrm{K}^{-1}$). The half-width of the localization radius is 0.03 radians (∼190km) for SIC DA and 0.1 radians (∼550km) for SIT DA, considering their different correlation length scales (Blanchard-Wrigglesworth & Bitz, 2014; Ponsoni et al., 2020). The SIC observational error is 10%, constant temporally and spatially, and the SITA observational error varies seasonally based on the spatial-mean of the Landy et al. (2022) SIT uncertainty (Fig. S1). The state variables updated by SIT DA are the SIC and SIT of each ice thickness category (SIC_N and SIT_N, respectively). SIC_N is the only variable that is updated by SIC DA due to the erroneous updates on SIT_N from SIC DA in some locations. An example is shown in Fig. S2, where some ensemble members have ice in the 5th category (> 1.1m) and their SIT_5 is above 1.1m, while other ensemble members do not have ice in this category. This bounded and nonlinear feature of SIT_N leads to a skewed relationship between the observed SIC and the state variable

SIT_5 and causes unrealistic updates on SIT_N. Updating SIT_N by SIC DA is also not recommended by previous studies (Kimmritz et al., 2018; Zhang et al., 2018, 2021) for similar reasons.

Three suites of reforecast experiments, SSTrest, SICDA and SITDA, using the SPEAR seasonal prediction system, are initialized on the first day of May, June, July, August, and September and run as 15-member one-year ensemble forecasts. The experiments share the same initial conditions in the atmosphere, land and ocean components, which are taken from the standard SPEAR_LO prediction system (Lu et al., 2020). SSTrest uses sea ice initial condition from SSTrest_IC, SICDA from SICDA_IC, and SITDA from SITDA_IC. More detailed information about the SPEAR reforecast configurations can be found in Zhang et al. (2022).

We decide to assimilate SITA instead of SIT mainly for two reasons. First, the model has a very different climatology from CryoSat-2 (Figs. S3a and c). We find that directly assimilating SIT reduces modeled SIT in the first few DA cycles in some grid cells and triggers thickness-based ice albedo feedback that further melts sea ice in those locations (figure not shown). Second, there is a large decrease in SIT from June to July in the observational data (Fig. S3c), which is caused by a sudden reduction in snow depth therefore unrealistically rapid unloading of snow load from the ice. However, the high anomaly correlation between SIV in the melting season and September SIE (Landy et al., 2022) suggests that the SITA observations contain valuable information for seasonal prediction.

2.4 Evaluation Metrics

We use the anomaly correlation coefficient (ACC) with observations to evaluate the model performance. Since there is no obvious trend in sea ice over our experiment time period (2011–2020), the full ACC is used. To test if two ACC values, ACC_1 and ACC_2, are significantly different, we apply a bootstrap procedure to get 1000 random samples (with replacement) of their ACC difference. If ACC_1 is greater than ACC_2, and the lower bound (5%) of the bootstrapped distribution of their difference is greater than zero, then we say ACC_1 is significantly greater than ACC_2, and vice versa. To compute an average ACC over time or space, we apply the Fisher-z transform to each correlation coefficient to get their z values, average the z values, and then apply an inverse transform to obtain the averaged correlation coefficient.

3 Results

3.1 Assimilation of SIT anomaly observations

We first analyze the time series of pan-Arctic SIV from SICDA_IC and SITDA_IC and compare it with CryoSat-2 (Fig. 1a). SICDA_IC can generally capture the sign of the SIV anomalies but fails to capture the interannual and seasonal variability, while SITDA_IC does a much better job at tracking the observed anomalies. The ACC of pan-Arctic SIV is increased from 0.46 to 0.89 due to the assimilation of SITA. The slight shift of SIV anomalies in SITDA_IC as compared to CryoSat-2 is mostly due to the 5-day DA cycle. The shift is largely reduced in an experiment with daily DA frequency (plot not shown). Looking at the ACC of SIV at grid-cell level, Fig. 1b shows that SICDA_IC simulates the SIV variability along the sea ice edges well, where the SIC component dominates the SIV variability. Conversely, SICDA_IC has zero or negative correlation with CryoSat-2 in the ice-covered Central Arctic, where SITDA_IC shows much higher ACC (Fig. 1c). The correlation difference map (Fig. 1d) confirms that SITDA_IC has similar ACC values to SICDA_IC in the marginal ice zones, and its major improvement is found in the Central Arctic. SSTrest_IC shows very similar SIV variability to SIC_IC (r=0.46; not shown),

which is expected since SIC DA has little impact on pan-Arctic SIV anomalies as stated in (Zhang et al., 2021).

3.2 Impact of SIT on seasonal predictions

We first evaluate the ACC of grid-cell SIC and SIE averaged over the Arctic for the target month of September from the three suites of reforecast experiments (Fig. 2). The evolution of skill as a function of forecasting days from different experiments follows a similar pattern in both metrics (Figs. 2a and c). SICDA and SITDA have an initial advantage over SSTrest (dashed lines) in the first month. SICDA (thin solid lines) has higher ACC than SITDA (thick solid lines) in the first ∼10 days in most experiments and gradually loses to SITDA as the forecasting day increases. To focus on the September-targeted forecast, SITDA is better than SICDA in the May-to-August initialized forecasts, but the improvement is only significant in the July and August initialized forecasts (Figs. 2b and d). SICDA is significantly more skillful than SITDA for September 1 initialized forecasts of SIC, and their skill is similar for local SIE. The mean skill of local SIC (SIE) averaged over all the initialization dates is 0.3(0.42) for SSTrest, 0.35(0.47) for SICDA, and 0.42(0.51) for SITDA. This suggests that the forecast skill of September local SIC and SIE is gradually improved by adding each observation, and the improvement from adding SIT DA is similar to the improvement from the early addition of SIC DA.

Fig. 3 shows the spatial map of the reforecast skill of all experiments. The skill from SSTrest and SICDA is negligible in the May-initialized runs and starts to emerge along the sea ice edge in June. SICDA has significantly higher ACC than SSTrest, mostly along the sea ice edges, for the September-initialized forecast (also shown in Fig. 2b). SITDA overall shows more positive ACC values (Fig. 3c) across the whole Arctic than SSTrest and SICDA. The difference map between SITDA and SICDA (Fig. 3d) highlights the skill improvement from adding SIT DA, which is most prominent in the Central Arctic and Fram Strait from the May-to-August initialized forecasts. Degradation is seen around the Chukchi Sea and part of the Beaufort in those months. The skill differences in the September-initialized forecasts is minor across the Arctic but overall SICDA has better SIC skill than SITDA.

To understand the differences in September SIC prediction skill across the reforecast experiments, we analyze the correlation between observed September SIC and the earlier SIV in their initial conditions, as a diagnostic for potential SIV-based predictability (Fig. 4). SSTrest_IC and SICDA_IC have very similar SIV-SIC correlation on the first day of May, June and July, with SICDA_IC showing slightly higher values than SSTrest_IC, thereafter. We find that the correlation is mostly positive along the sea ice edge in SICDA_IC and negative in the Central Arctic until September (Fig. 4b). The correlation in CryoSat-2 (Fig. 4d) has similar positive patterns near the ice edge but has more positive values in the Central Arctic, which leads to overall higher pan-Arctic averaged values (see text on each panel). SITDA_IC has higher pan-Arctic averaged correlation than CryoSat-2 for May, June, July, and August (Fig. 4c), indicating that it combines the advantages of the model and both observation types. Fig. 4e, which plots the correlation differences between SITDA_IC and SICDA_IC, shows notable improvements from SIT DA in the Central Arctic and GIN Seas. The differences are significant for all months. However, degradation is seen in the Chukchi Sea and part of the Beaufort Sea, where SICDA_IC has neutral or slightly positive correlation but CryoSat-2 has negative correlation for May, June, and July. As a consequence, SITDA_IC has negative correlation values around the Chukchi Sea for those initialization dates. This is important for seasonal sea ice prediction because the September SIE contour is typically located over this region of anticorrelation in the Chukchi Sea (Fig. 4e). The difference map of the SIV-SIC correlation shows a very similar pattern to the skill difference map between SITDA and SICDA (Fig. 3d), with prominent improvements seen in the Central Arctic and degradation around the

Chukchi and Beaufort Seas. Their pattern correlations for all months are significantly positive, and are above 0.5 for the months of May, June, and July. This suggests that improvement/degradation in prediction skill is more likely to appear in regions where the SIV-SIC correlation is improved/degraded, especially at long lead times.

To assess if the negative SIV-SIC correlation is unique over the CryoSat-2 era 2011-2020, we first look at correlation maps computed over different decades from the SICDA_IC experiment, which was run over a longer period of 1991-2020 due to observational availability (Fig. S4). We find that the negative regions of SIV-SIC correlation are only present in some decades and are not present over the longer time period (30 years). For instance, Arctic-averaged correlation between June SIV and September SIC was 0.4 in the 2000s compared to 0.05 in the 2010s. We also performed a similar analysis using a large (30 member) ensemble of SPEAR_LO CMIP6 historical forcing simulations. Although the ensemble mean shows a homogenous positive SIV-SIC map, the correlation values vary greatly amongst members (Fig. S5). Regions of negative SIV-SIC correlation are seen in most ensemble members in varying spatial locations. We calculate the percentage of area that has negative SIV-SIC correlation values from different experiments (Table S1) and confirm that the SPEAR_LO ensemble has a large range of negative area. All DA experiments are within this range, as well as the CryoSat-2 observations, which always have less negative area than SICDA_IC. This indicates that the SIV-SIC correlation computed over a 10-year period has a large natural variability, and the negative values seen in CryoSat-2 are within this variability. According to the CryoSat-2 observations, the negative values for the 2010s are located around the Chukchi Sea. It is also possible that the CryoSat-2 observations have errors in this area. We decompose the SIV-SIC correlation from CryoSat-2 into the freeboard-SIC and snow depth-SIC correlations and find that negative values are found in both of the component correlations as well. Further investigations into the freeboard retrieval and snow depth estimates are necessary to understand the cause of the negative SIV-SIC correlations but it is outside the scope of this study.

We also evaluate the forecast skill of regional SIE and correspondingly examine the correlation between the observed September SIE and earlier SIV. SITDA shows better skill than SICDA in the Laptev and East Siberian Seas (Figs. S6a and b) and worse skill in the Chukchi Sea and Canadian Archipelago (Figs. S6c and e). The improvement/degradation in the overall forecast skill can mostly be explained by the improvement/degradation in their regional SIV-SIE correlations. SICDA_IC matches well with the observations in the Laptev and Beaufort Seas (Figs. S6a and d) and performs poorly in the East Siberian Sea (Fig. S6b), where the SITDA_IC shows the greatest advantage. The observed SIV-SIE correlation in the Chukchi Sea drops abruptly from August to July and is even negative in June and earlier. This is also where the negative local SIV-SIC correlation exists in Fig. 4c. As suggested in Fig. S4, this is likely unique to the 2010s, when the SIV-SIE/SIC correlation is disrupted by other factors, e.g., storms happening in the western Arctic during the melting season (Parkinson & Comiso, 2013; Lukovich et al., 2021). This negative correlation does not appear in the Chukchi Sea in SICDA_IC, except for the July lead (Fig. S4c) and hence assimilating CryoSat-2 actually reduces the SIV-SIE correlation significantly in this region (Fig. S6c). The results for the pan-Arctic SIE are more equivocal, in that although SITDA_IC has higher SIV-SIE correlation values than SICDA_IC on all intialization dates (compare solid red to solid blue lines), we only see significant improvements in the August and September-initialized forecasts and significant degradation in the June-initialized forecast (compare red and blue dots).

To better understand the June forecast skill in SITDA and SICDA, we compare the SIV-SIE and SIE-SIE correlations at pan-Arctic scale in their initial conditions (i.e., SITDA_IC and SICDA_IC) from 2011 to 2020 (Figs. S7a and b) and find that the SIE-SIE correlation has a local maximum near mid-June after the initial drop, which is even greater than the SIV-SIE correlation. This feature is not seen in the longer time period

(Fig. S7c). The comparison between Figs. S7b and c suggests that the June SIV-SIE correlation is abnormally low and the June SIE-SIE correlation is abnormally high in the 2010s compared to their values in the climatology. This feature may help explain why the pan-Arctic June SIV is not a strong predictor of the pan-Arctic September SIE in the 2010s.

4 Conclusions and Discussion

In this study, we assimilate the first year-round sea ice thickness (SIT) observations retrieved from the CryoSat-2 satellite radar altimeter into the GFDL ocean and sea ice model (MOM6/SIS2) through our sea ice data assimilation framework built upon DART and SIS2. Considering that our model has a very different SIT climatology from CryoSat-2, and the observations have an unrealistically fast mean thickness drop from June to July due to problems in the snow depth estimates, we assimilate the SIT anomalies (SITA) instead of the original SIT. To counteract the large uncertainty in SIT retrievals resulting from snow depth uncertainty, we plan to directly assimilate freeboard retrievals from CryoSat-2 in the near future.

Our DA results over the period 2011–2020 show that the pan-Arctic and regional sea ice volume anomalies are significantly improved when SIT is assimilated. The grid-cell scale evaluation show that the improvements occur mainly in the Central Arctic. We conduct three suites of reforecast experiments, SSTrest that has no direct sea ice DA in initialization, SICDA that includes assimilation of SIC, and SITDA that has joint assimilation of SIC and SIT. The evaluation of grid-cell SIC and SIE shows that SITDA has better skill in predicting September sea ice than SICDA in the May to August-initialized forecasts, although only the July and August-initialized forecasts have passed the 95% significance test. The skill improvement is mostly found in the Central Arctic and GIN Seas. Degradation is seen around the Chukchi Sea, part of the Beaufort and East Siberian Seas. The mean skill averaged over all initialization months for the three experiments suggest that the additional improvement on September sea ice forecast brought by SIT DA is comparable to the earlier addition of SIC DA.

We hypothesize that the skill improvements from assimilating SIT is mainly due to the SIV-based predictability change. We analyze the correlation between September SIC and earlier SIV in the different initial conditions for diagnosis. The SIV-SIC correlation difference between SITDA and SICDA initial conditions closely mirrors the September SIC prediction skill differences between these experiments. CryoSat-2 has a region of negative SIV-SIC correlation around the Chukchi Sea. As a result of assimilating CryoSat-2 SITA, SITDA_IC has negative SIV-SIC correlation values around the same area, while it has higher SIV-SIC correlation values than SICDA_IC almost everywhere else, especially in the Central Arctic. We compute the SIV-SIC correlation in different decades using the SICDA initial conditions and find that the correlation is positive across the whole Arctic over a longer time period (30 years) but can have negative values in some decades. We also show this negative SIV-SIC correlation feature is seen in most ensemble members of SPEAR_LO, at varying spatial locations, which suggests that the SIV-SIC correlation has a large natural variability and there is not an obvious single or set of regions where we can choose to discard the observations. On the other hand, it is also possible that the CryoSat-2 observations have errors around the Chukchi Sea, and assimilating these data causes lower September SIC forecast skill in the area. Further observational studies are needed to assess and potentially improve the quality of the CryoSat-2 observations on a regional basis.

The pan-Arctic SIE results are more complicated. Although the SIV-based predictability of September SIE is clearly improved in the initial condition of SITDA in all months, statistically significant improvement in the actual September sea ice skill is only seen in the August- and September-initialized forecasts. SITDA loses to SICDA significantly in

the June-initialized forecast, which is very likely due to the disrupted SIV-SIC correlation in the Chukchi and Beaufort area and to the enhanced impact ("bump") of June SIC correlations in the 2010s.

Our results are limited by the length of the available SIT data, and hence should be interpreted with caution. The September Arctic sea ice in the 2010s decade is found to be particularly hard to predict at longer lead times because it seems to have a weaker correlation with its dominant predictor: the SIV anomaly in the melt season. In SICDA experiments the SIV-SIC correlations are significantly weaker in the 2010s compared to the 2000s. Nevertheless, we find unique value of the CryoSat-2 SIT observations for improving the Arctic summer sea ice prediction at longer lead times. Our study therefore suggests that having a longer record of satellite-retrieved SIT observations is critical for the seasonal prediction of Arctic summer sea ice.

5 Data Availability Statement

Our model outputs including sea ice thickness and concentration from the data assimilation experiments and the reforecast experiments are shared at 10.6084/m9.figshare.23646360. The year-round CryoSat-2 sea ice thickness observations can be downloaded at https://data.bas.ac.uk/full-record.php?id=GB/NERC/BAS/PDC/01613. The NSIDC NASA Team sea ice concentration observations can be downloaded at https://nsidc.org/data/nsidc-0051/versions/2.

Acknowledgments

Yong-Fei Zhang received award NA18OAR4320123 under the Cooperative Institute for Modeling the Earth System (CIMES) at Princeton University, and the National Oceanic and Atmospheric Administration, U.S. Department of Commerce. We thank Feiyu Lu for providing ocean initial conditions and Xiaosong Yang for preparing SST observations.

References

Anderson, J. L. (2001, December). An ensemble adjustment kalman filter for data assimilation. *Monthly Weather Review*, *129*(12), 2884-2903.

Blanchard-Wrigglesworth, E., Armour, K. C., Bitz, C. M., & DeWeaver, E. (2011). Persistence and inherent predictability of arctic sea ice in a gcm ensemble and observations. *Journal of Climate*, *24*(1), 231–250.

Blanchard-Wrigglesworth, E., & Bitz, C. M. (2014). Characteristics of arctic sea-ice thickness variability in gcms. *Journal of Climate*, *27*(21), 8244–8258.

Blockley, E. W., & Peterson, K. A. (2018). Improving met office seasonal predictions of arctic sea ice using assimilation of cryosat-2 thickness. *The Cryosphere*, *12*(11), 3419–3438.

Bonan, D. B., Bushuk, M., & Winton, M. (2019). A spring barrier for regional predictions of summer arctic sea ice. *Geophysical Research Letters*, *46*(11), 5937–5947.

Briegleb, P., & Light, B. (2007). A delta-eddington mutiple scattering parameterization for solar radiation in the sea ice component of the community climate system model.

Bushuk, M., Msadek, R., Winton, M., Vecchi, G. A., Gudgel, R., Rosati, A., & Yang, X. (2017). Skillful regional prediction of arctic sea ice on seasonal timescales. *Geophysical Research Letters*, *44*(10), 4953–4964.

Bushuk, M., Winton, M., Bonan, D. B., Blanchard-Wrigglesworth, E., & Delworth, T. L. (2020). A mechanism for the arctic sea ice spring predictability barrier. *Geophysical Research Letters*, *47*(13), e2020GL088335.

Bushuk, M., Yang, X., Winton, M., Msadek, R., Harrison, M., Rosati, A., & Gudgel, R. (2019). The value of sustained ocean observations for sea ice predictions in

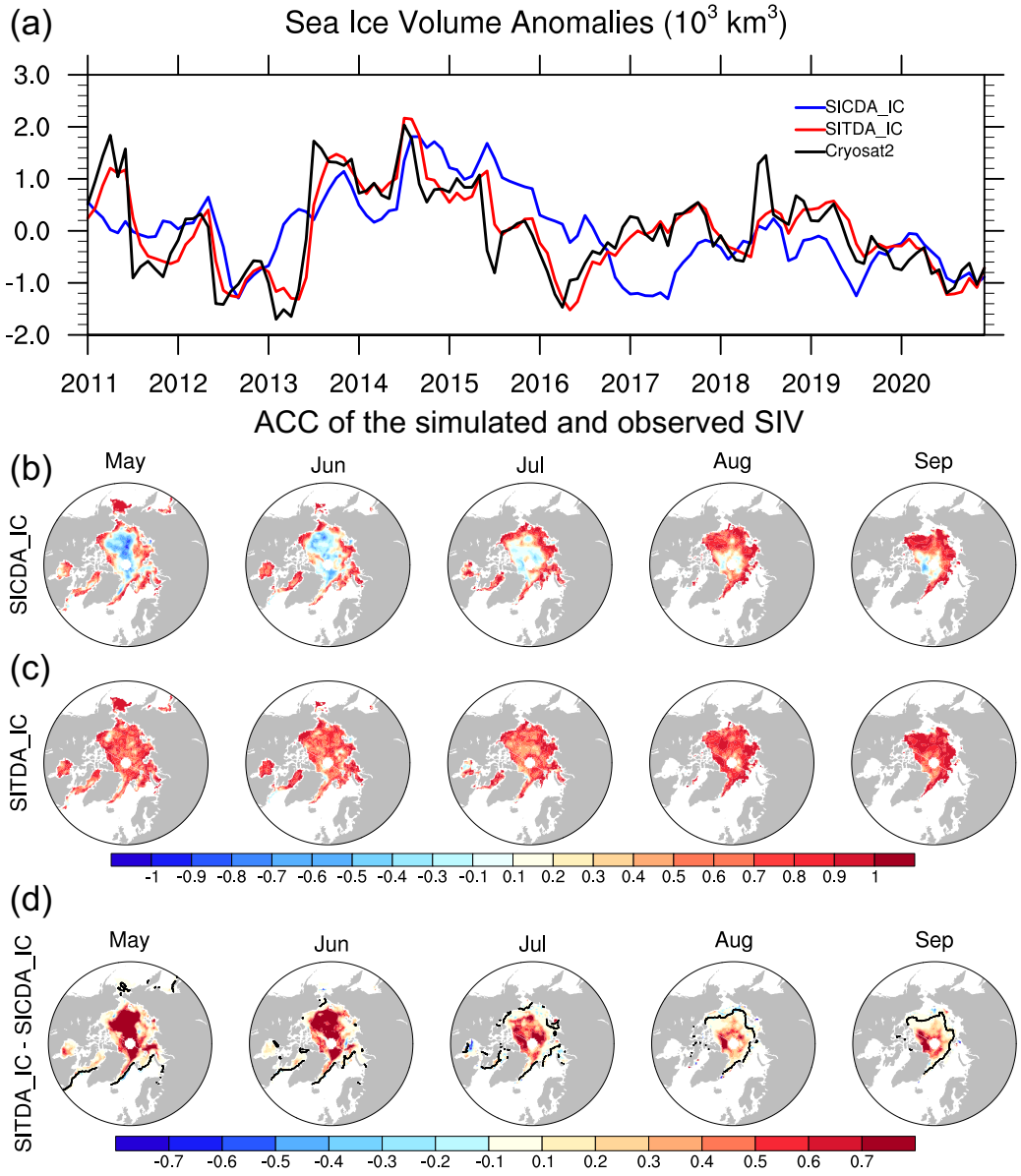

Figure 1. Comparison between the two DA experiments. (a) The time series of sea ice volume anomalies for SICDA_IC (blue), SITDA_IC (red), and observations (black). The spatial map of the ACC of simulated and observed SIV for (b) SICDA_IC, (c) SITDA_IC, and (d) their difference (SITDA_IC - SICDA_IC). The black contours on (d) are the observed SIE climatology over 2011-2020.

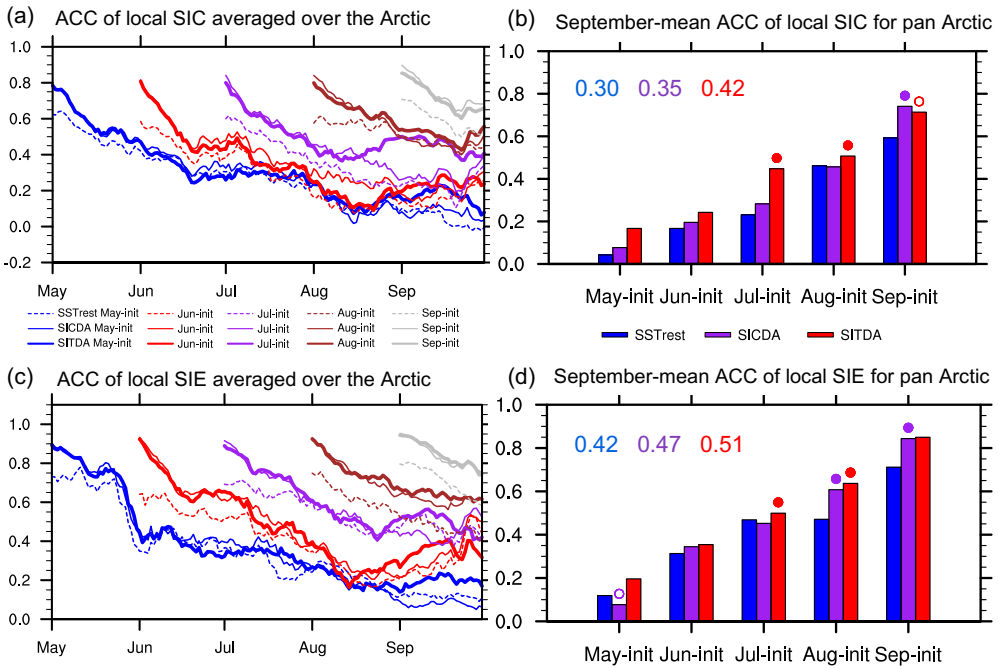

Figure 2. Pan-Arctic averaged ACC of (a) local SIC and (c) local SIE as a function of forecast days, and the September-mean ACC of (b) local SIC and (d) local SIE from each initialization month. Prediction skill is shown for the SSTrest (dashed lines), SICDA (thin solid lines), and SITDA (thick solid lines) reforecast experiments. For each grid cell, the local SIE is one if SIC >15% and zero if SIC <15%. ACC is calculated every day of the year using data from 2011-2020. Only grid cells that have >10% SIC interannual variability are taken into average for each day. The purple dots in (b) and (d) indicate that SICDA is significantly better than SSTrest, and the red dots/circles that SITDA/SICDA is significantly better than SICDA/SITDA. The numbers in (b) and (d) indicate the mean ACC over all the initialization months for SSTrest (blue), SICDA (purple), and SITDA (red).

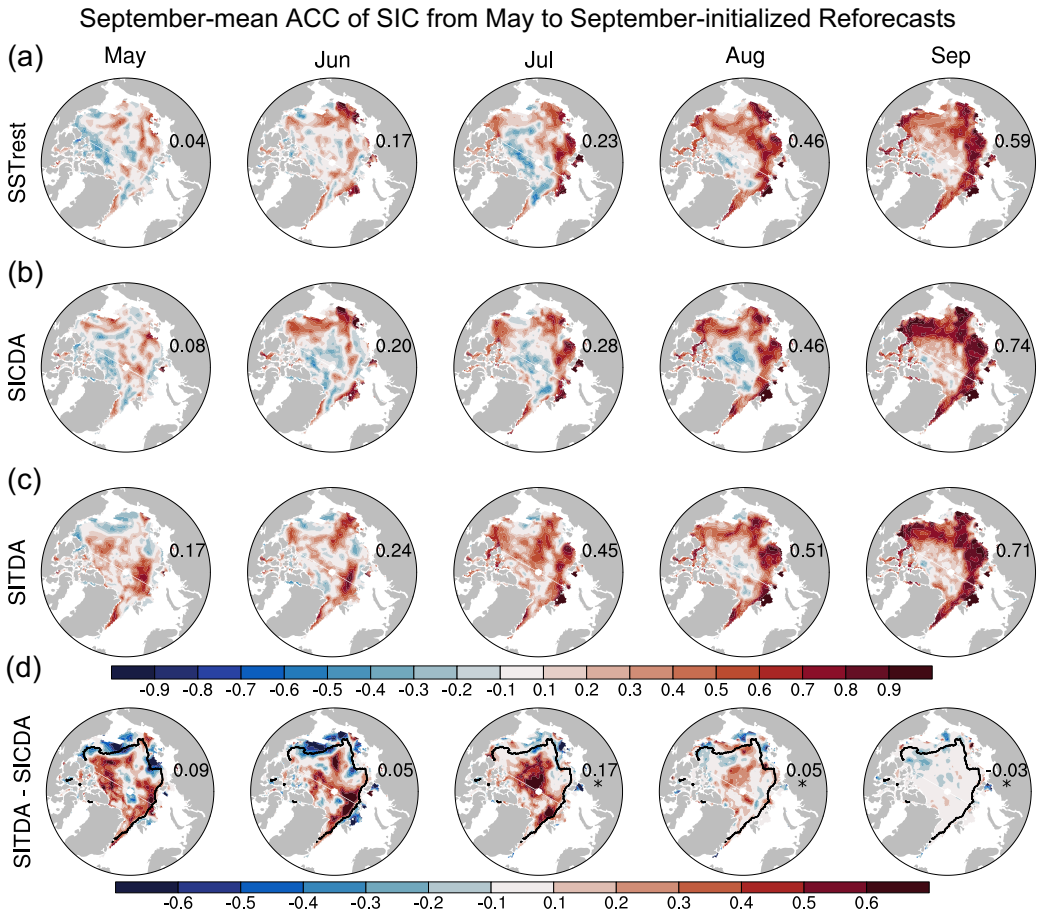

Figure 3. Correlation between the observed September SIC and the forecasted September SIC initialized from May to September from (a) SSTrest, (b) SICDA, (c) SITDA, and (d) the difference between the two DA-initialized reforecast experiments (SITDA - SICDA). The number on each plot is the pan-Arctic area-weighted average of SIC ACC excluding the grid cells where the observed SIC interannual standard deviation is lower than 10% or there is no observation. The numbers with asterisk on (d) indicate that the differences between SITDA and SICDA passed the 95% significance test.

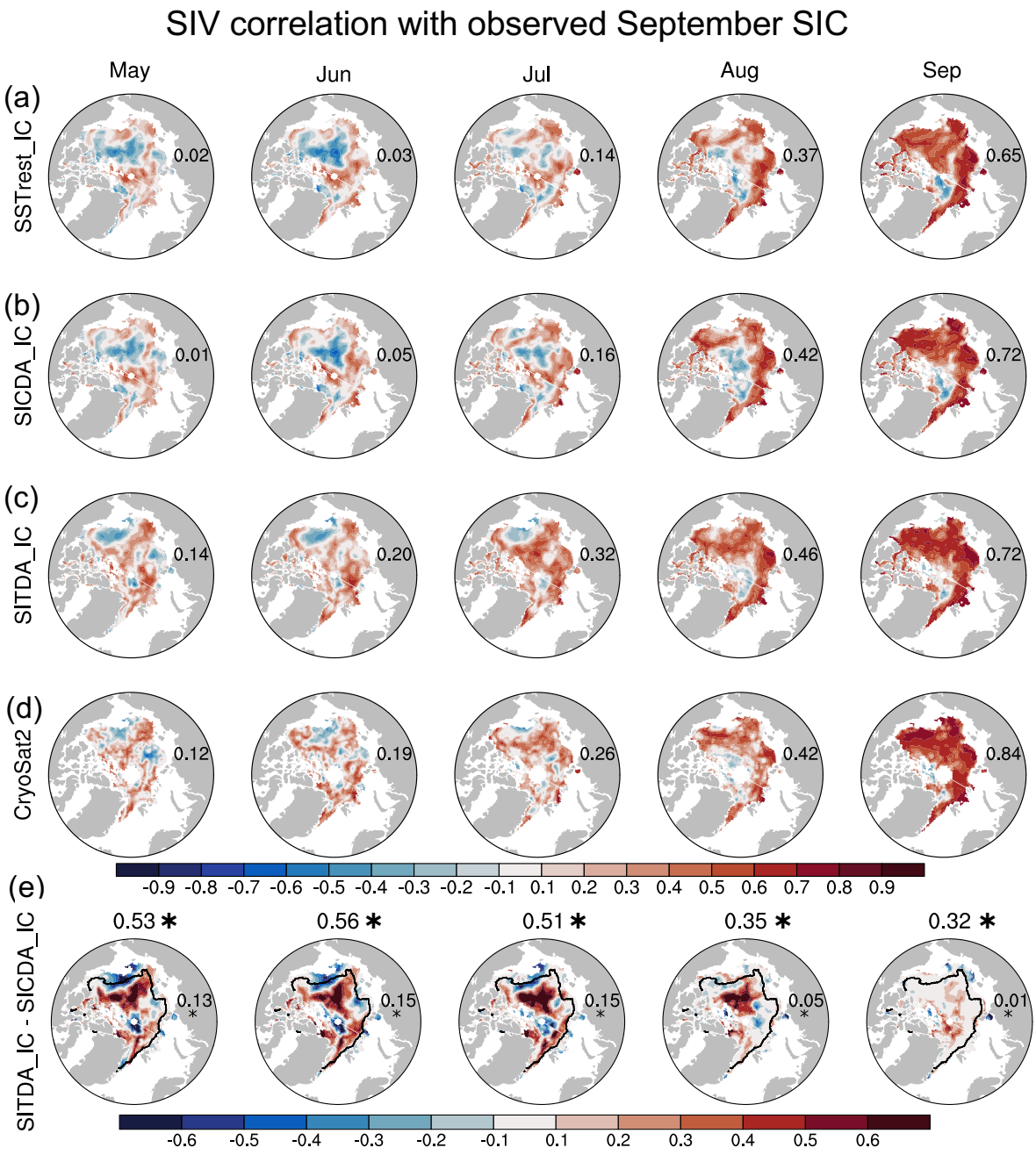

Figure 4. Correlation between the observed September SIC and SIV from the 1st day of May, June, July, August, and September for (a) SSTrest_IC, (b) SICDA_IC, (c) SITDA_IC, and (d) CryoSat-2, and (e) the difference between the two DA experiments (SITDA_IC - SICDA_IC). The correlation is calculated for every day in September and is then averaged over 30 days. The number on each map is the pan-Arctic area-weighted average correlation excluding the grid cells where the observed SIC interannual standard deviation is lower than 10% or there is no observation. The numbers with asterisk on the maps in (e) indicate that the differences between SITDA_IC and SICDA_IC passed the 95% significance test. The numbers above each map in (e) are the pattern correlations between (e) and Fig. 3d and the asterisk indicates that the correlation is 95% significantly positive.

the barents sea. *Journal of Climate*, *32*(20), 7017–7035.

Bushuk, M., Zhang, Y., Winton, M., Hurlin, B., Delworth, T., Lu, F., ... others (2022). Mechanisms of regional arctic sea ice predictability in two dynamical seasonal forecast systems. *Journal of Climate*, 1–63.

Cavalieri, D. J., Parkinson, C. L., Gloersen, P., & Zwally, H. J. (1996). *Sea Ice Concentrations from Nimbus-7 SMMR and DMSP SSM/I-SSMIS Passive Microwave Data, Version 1.* Boulder, Colorado USA. Retrieved from `https://doi.org/10.5067/8GQ8LZQVL0VL`

Caya, A., Buehner, M., & Carrieres, T. (2010). Analysis and forecasting of sea ice conditions with three-dimensional variational data assimilation and a coupled ice–ocean model. *Journal of Atmospheric and Oceanic Technology*, *27*(2), 353–369.

Chen, Z., Liu, J., Song, M., Yang, Q., & Xu, S. (2017). Impacts of assimilating satellite sea ice concentration and thickness on arctic sea ice prediction in the ncep climate forecast system. *Journal of Climate*, *30*(21), 8429–8446.

Chevallier, M., y Mélia, D. S., Voldoire, A., Déqué, M., & Garric, G. (2013). Seasonal forecasts of the pan-arctic sea ice extent using a gcm-based seasonal prediction system. *Journal of Climate*, *26*(16), 6092–6104.

Dai, P., Gao, Y., Counillon, F., Wang, Y., Kimmritz, M., & Langehaug, H. R. (2020). Seasonal to decadal predictions of regional arctic sea ice by assimilating sea surface temperature in the norwegian climate prediction model. *Climate Dynamics*, *54*(9-10), 3863–3878.

Dawson, G., Landy, J., Tsamados, M., Komarov, A. S., Howell, S., Heorton, H., & Krumpen, T. (2022). A 10-year record of arctic summer sea ice freeboard from cryosat-2. *Remote Sensing of Environment*, *268*, 112744.

Delworth, T. L., Cooke, W. F., Adcroft, A., Bushuk, M., Chen, J.-H., Dunne, K. A., ... others (2020). SPEAR: The next generation GFDL modeling system for seasonal to multidecadal prediction and projection. *Journal of Advances in Modeling Earth Systems*, *12*(3), e2019MS001895.

Dirkson, A., Denis, B., & Merryfield, W. (2019). A multimodel approach for improving seasonal probabilistic forecasts of regional arctic sea ice. *Geophysical Research Letters*, *46*(19), 10844–10853.

Fritzner, S., Graversen, R., Christensen, K. H., Rostosky, P., & Wang, K. (2019). Impact of assimilating sea ice concentration, sea ice thickness and snow depth in a coupled ocean–sea ice modelling system. *The Cryosphere*, *13*(2), 491–509.

Hibler, W. D. (1979). A dynamic thermodynamic sea ice model. *Journal of physical oceanography*, *9*(4), 815–846.

Kimmritz, M., Counillon, F., Bitz, C., Massonnet, F., Bethke, I., & Gao, Y. (2018). Optimising assimilation of sea ice concentration in an earth system model with a multicategory sea ice model. *Tellus A: Dynamic Meteorology and Oceanography*, *70*(1), 1–23.

Kimmritz, M., Counillon, F., Smedsrud, L. H., Bethke, I., Keenlyside, N., Ogawa, F., & Wang, Y. (2019). Impact of ocean and sea ice initialisation on seasonal prediction skill in the arctic. *Journal of Advances in Modeling Earth Systems*, *11*(12), 4147–4166.

Kwok, R., & Cunningham, G. (2008). Icesat over arctic sea ice: Estimation of snow depth and ice thickness. *Journal of Geophysical Research: Oceans*, *113*(C8).

Landy, J. C., Dawson, G. J., Tsamados, M., Bushuk, M., Stroeve, J. C., Howell, S. E., ... others (2022). A year-round satellite sea-ice thickness record from cryosat-2. *Nature*, *609*(7927), 517–522.

Laxon, S. W., Giles, K. A., Ridout, A. L., Wingham, D. J., Willatt, R., Cullen, R., ... others (2013). Cryosat-2 estimates of arctic sea ice thickness and volume. *Geophysical Research Letters*, *40*(4), 732–737.

Lindsay, R., & Zhang, J. (2006). Assimilation of ice concentration in an ice–ocean model. *Journal of Atmospheric and Oceanic Technology*, *23*(5), 742–749.

Lisæter, K. A., Rosanova, J., & Evensen, G. (2003). Assimilation of ice concentration in a coupled ice–ocean model, using the ensemble kalman filter. *Ocean Dynamics*, *53*(4), 368–388.

Liston, G. E., Itkin, P., Stroeve, J., Tschudi, M., Stewart, J. S., Pedersen, S. H., ... Elder, K. (2020). A lagrangian snow-evolution system for sea-ice applications (snowmodel-lg): Part i—model description. *Journal of Geophysical Research: Oceans*, *125*(10), e2019JC015913.

Lu, F., Harrison, M. J., Rosati, A., Delworth, T. L., Yang, X., Cooke, W. F., ... others (2020). GFDL's SPEAR seasonal prediction system: Initialization and ocean tendency adjustment (OTA) for coupled model predictions. *Journal of Advances in Modeling Earth Systems*, *12*(12), e2020MS002149.

Lukovich, J. V., Stroeve, J. C., Crawford, A., Hamilton, L., Tsamados, M., Heorton, H., & Massonnet, F. (2021). Summer extreme cyclone impacts on arctic sea ice. *Journal of Climate*, *34*(12), 4817–4834.

Massonnet, F., Fichefet, T., & Goosse, H. (2015). Prospects for improved seasonal arctic sea ice predictions from multivariate data assimilation. *Ocean Modelling*, *88*, 16–25.

Meier, W. N., Hovelsrud, G. K., Van Oort, B. E., Key, J. R., Kovacs, K. M., Michel, C., ... others (2014). Arctic sea ice in transformation: A review of recent observed changes and impacts on biology and human activity. *Reviews of Geophysics*, *52*(3), 185–217.

Merryfield, W., Lee, W.-S., Wang, W., Chen, M., & Kumar, A. (2013). Multi-system seasonal predictions of arctic sea ice. *Geophysical Research Letters*, *40*(8), 1551–1556.

Mu, L., Yang, Q., Losch, M., Losa, S. N., Ricker, R., Nerger, L., & Liang, X. (2018). Improving sea ice thickness estimates by assimilating cryosat-2 and smos sea ice thickness data simultaneously. *Quarterly Journal of the Royal Meteorological Society*, *144*(711), 529–538.

Parkinson, C. L., & Comiso, J. C. (2013). On the 2012 record low arctic sea ice cover: Combined impact of preconditioning and an august storm. *Geophysical Research Letters*, *40*(7), 1356–1361.

Peterson, K. A., Arribas, A., Hewitt, H., Keen, A., Lea, D., & McLaren, A. (2015). Assessing the forecast skill of arctic sea ice extent in the glosea4 seasonal prediction system. *Climate Dynamics*, *44*, 147–162.

Petty, A. A., Kurtz, N. T., Kwok, R., Markus, T., & Neumann, T. A. (2020). Winter arctic sea ice thickness from icesat-2 freeboards. *Journal of Geophysical Research: Oceans*, *125*(5), e2019JC015764.

Ponsoni, L., Massonnet, F., Docquier, D., Van Achter, G., & Fichefet, T. (2020). Statistical predictability of the arctic sea ice volume anomaly: identifying predictors and optimal sampling locations. *The Cryosphere*, *14*(7), 2409–2428.

Reynolds, R. W., Smith, T. M., Liu, C., Chelton, D. B., Casey, K. S., & Schlax, M. G. (2007). Daily high-resolution-blended analyses for sea surface temperature. *Journal of climate*, *20*(22), 5473–5496.

Sigmond, M., Fyfe, J., Flato, G., Kharin, V., & Merryfield, W. (2013). Seasonal forecast skill of arctic sea ice area in a dynamical forecast system. *Geophysical Research Letters*, *40*(3), 529–534.

Sigmond, M., Reader, M., Flato, G., Merryfield, W., & Tivy, A. (2016). Skillful seasonal forecasts of arctic sea ice retreat and advance dates in a dynamical forecast system. *Geophysical Research Letters*, *43*(24), 12–457.

Stroeve, J., & Notz, D. (2018). Changing state of arctic sea ice across all seasons. *Environmental Research Letters*, *13*(10), 103001.

Tian-Kunze, X., Kaleschke, L., Maaß, N., Mäkynen, M., Serra, N., Drusch, M., & Krumpen, T. (2014). Smos-derived thin sea ice thickness: algorithm baseline, product specifications and initial verification. *The Cryosphere*, *8*(3), 997–1018.

Tietsche, S., Notz, D., Jungclaus, J., & Marotzke, J. (2013). Assimilation of sea-ice concentration in a global climate model–physical and statistical aspects. *Ocean science*, *9*(1), 19–36.

Tsujino, H., Urakawa, S., Nakano, H., Small, R. J., Kim, W. M., Yeager, S. G., ... others (2018). Jra-55 based surface dataset for driving ocean–sea-ice models (jra55-do). *Ocean Modelling*, *130*, 79–139.

Van Woert, M. L., Zou, C.-Z., Meier, W. N., Hovey, P. D., Preller, R. H., & Posey, P. G. (2004). Forecast verification of the polar ice prediction system (pips) sea ice concentration fields. *Journal of Atmospheric and Oceanic Technology*, *21*(6), 944–957.

Xie, J., Counillon, F., Bertino, L., Tian-Kunze, X., & Kaleschke, L. (2016). Benefits of assimilating thin sea ice thickness from smos into the topaz system. *The Cryosphere*, *10*(6), 2745–2761.

Yang, Q., Losa, S. N., Losch, M., Tian-Kunze, X., Nerger, L., Liu, J., ... Zhang, Z. (2014). Assimilating smos sea ice thickness into a coupled ice-ocean model using a local seik filter. *Journal of Geophysical Research: Oceans*, *119*(10), 6680–6692.

Zeng, J., Yang, Q., Li, X., Yuan, X., Bushuk, M., & Chen, D. (2023). Reducing the spring barrier in predicting summer arctic sea ice concentration. *Geophysical Research Letters*, *50*(8), e2022GL102115.

Zhang, Y.-F., Bitz, C. M., Anderson, J. L., Collins, N., Hendricks, J., Hoar, T., ... Massonnet, F. (2018). Insights on sea ice data assimilation from perfect model observing system simulation experiments. *Journal of Climate*, *31*(15), 5911–5926.

Zhang, Y.-F., Bushuk, M., Winton, M., Hurlin, B., Delworth, T., Harrison, M., ... Yang, X. (2022). Subseasonal-to-seasonal arctic sea ice forecast skill improvement from sea ice concentration assimilation. *Journal of Climate*, 1–48.

Zhang, Y.-F., Bushuk, M., Winton, M., Hurlin, B., Yang, X., Delworth, T., & Jia, L. (2021). Assimilation of satellite-retrieved sea ice concentration and prospects for september predictions of arctic sea ice. *Journal of Climate*, *34*(6), 2107–2126.

Figure1.

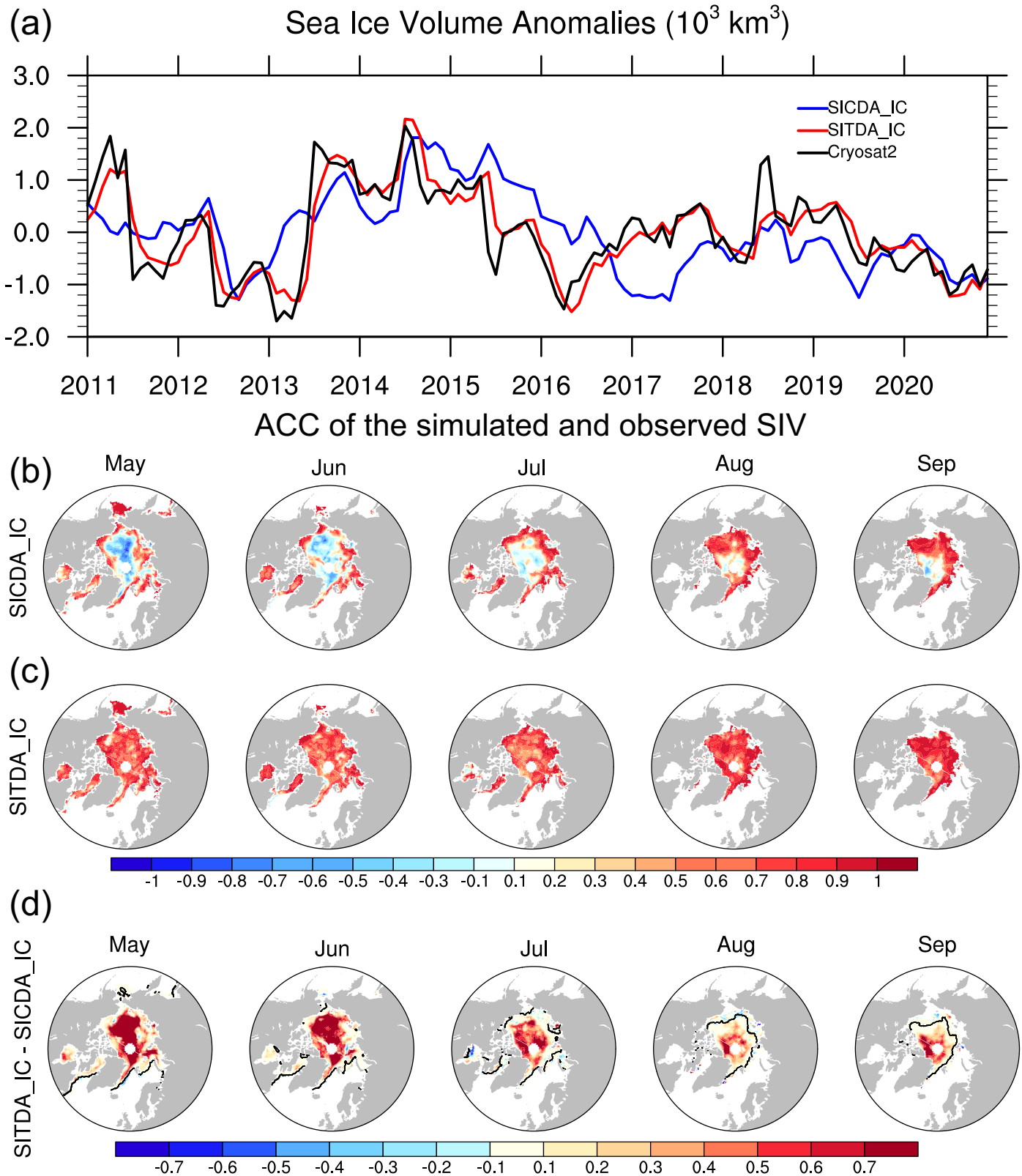
(a)
Sea Ice Volume Anomalies (10^3 km^3)
3.0
2.0
1.0
0.0
-1.0
-2.0
SICDA_IC
SITDA_IC
Cryosat2
2011
2012
2013
2014
2015
2016
2017
2018
2019
2020
ACC of the simulated and observed SIV
(b)
May
Jun
Jul
Aug
Sep
SICDA_IC
(c)
SITDA_IC
-1 -0.9 -0.8 -0.7 -0.6 -0.5 -0.4 -0.3 -0.1 0.1 0.2 0.3 0.4 0.5 0.6 0.7 0.8 0.9 1
(d)
May
Jun
Jul
Aug
Sep
SITDA_IC - SICDA_IC
-0.7 -0.6 -0.5 -0.4 -0.3 -0.2 -0.1 0.1 0.2 0.3 0.4 0.5 0.6 0.7

Figure2.

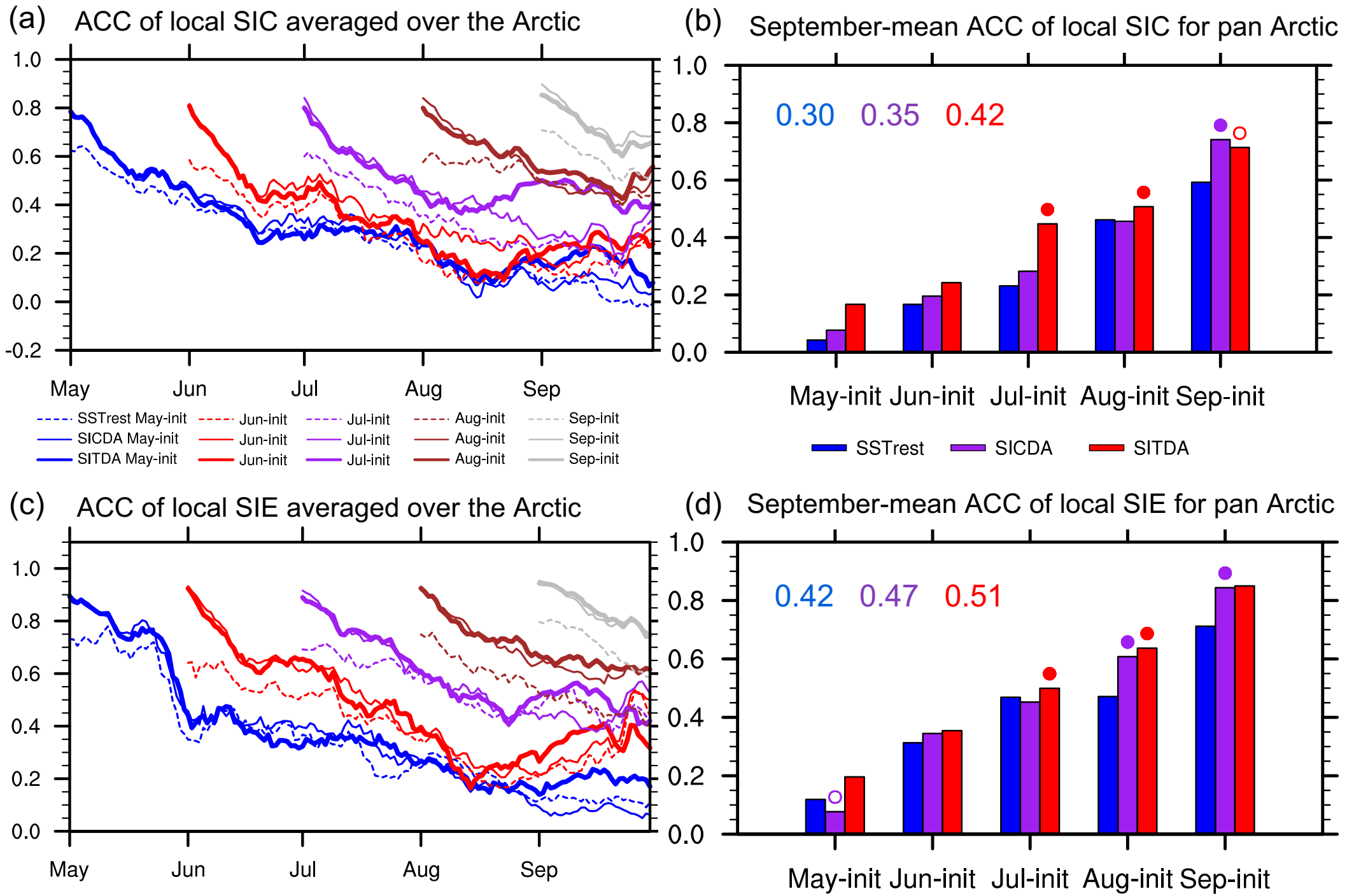
(a)
ACC of local SIC averaged over the Arctic
1.0
0.8
0.6
0.4
0.2
0.0
-0.2
May
Jun
Jul
Aug
Sep
SSTrest May-init
SICDA May-init
SITDA May-init
Jun-init
Jun-init
Jun-init
Jul-init
Jul-init
Jul-init
Aug-init
Aug-init
Aug-init
Sep-init
Sep-init
Sep-init
(b)
September-mean ACC of local SIC for pan Arctic
0.30
0.35
0.42
May-init
Jun-init
Jul-init
Aug-init
Sep-init
SSTrest
SICDA
SITDA
(c)
ACC of local SIE averaged over the Arctic
(d)
September-mean ACC of local SIE for pan Arctic
0.42
0.47
0.51

Figure3.

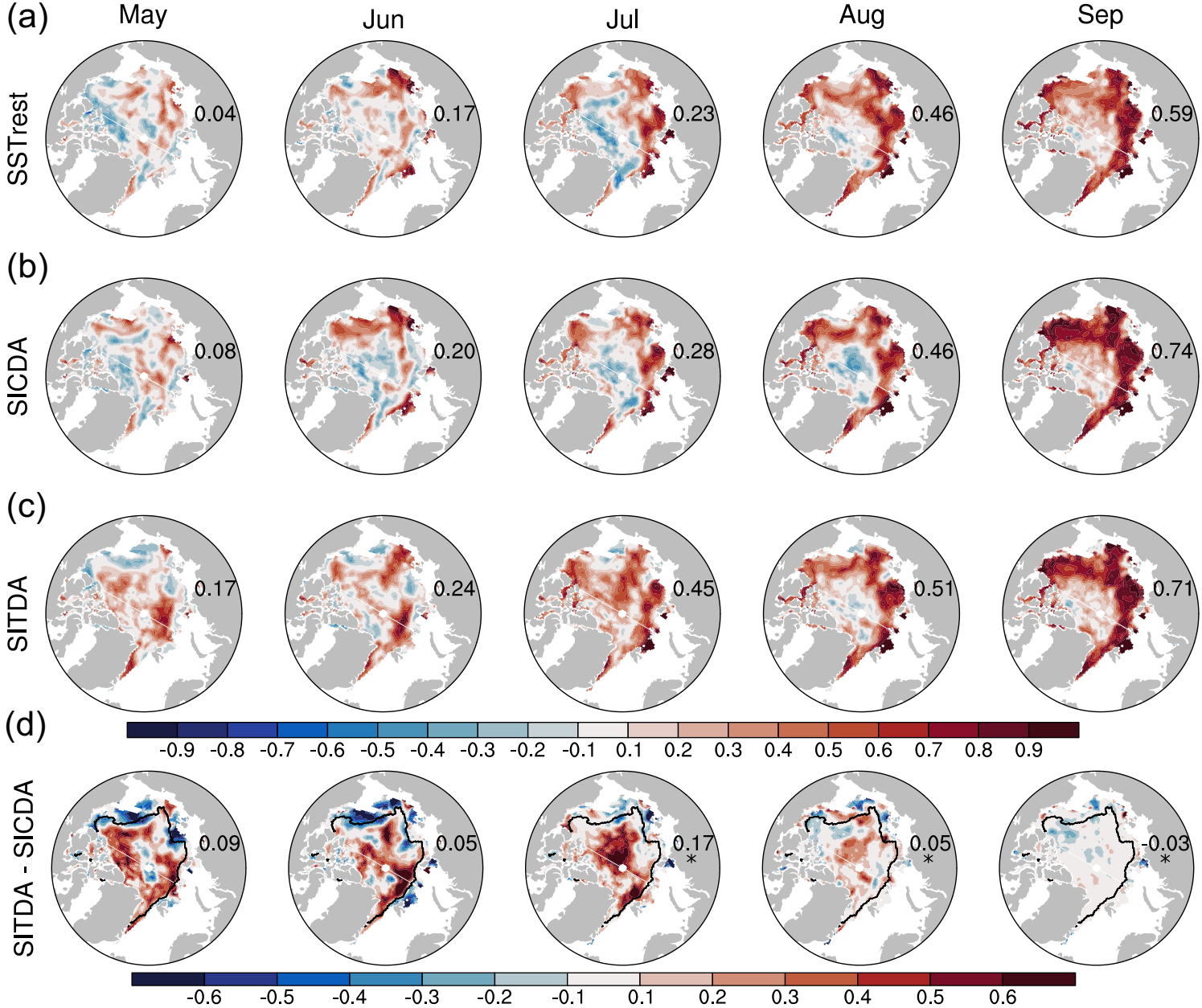
September-mean ACC of SIC from May to September-initialized Reforecasts
(a)
May
Jun
Jul
Aug
Sep
SSTrest
0.04
0.17
0.23
0.46
0.59
(b)
SICDA
0.08
0.20
0.28
0.46
0.74
(c)
SITDA
0.17
0.24
0.45
0.51
0.71
(d)
-0.9 -0.8 -0.7 -0.6 -0.5 -0.4 -0.3 -0.2 -0.1 0.1 0.2 0.3 0.4 0.5 0.6 0.7 0.8 0.9
SITDA - SICDA
0.09
0.05
0.17 *
0.05 *
-0.03 *
-0.6 -0.5 -0.4 -0.3 -0.2 -0.1 0.1 0.2 0.3 0.4 0.5 0.6

Figure4.

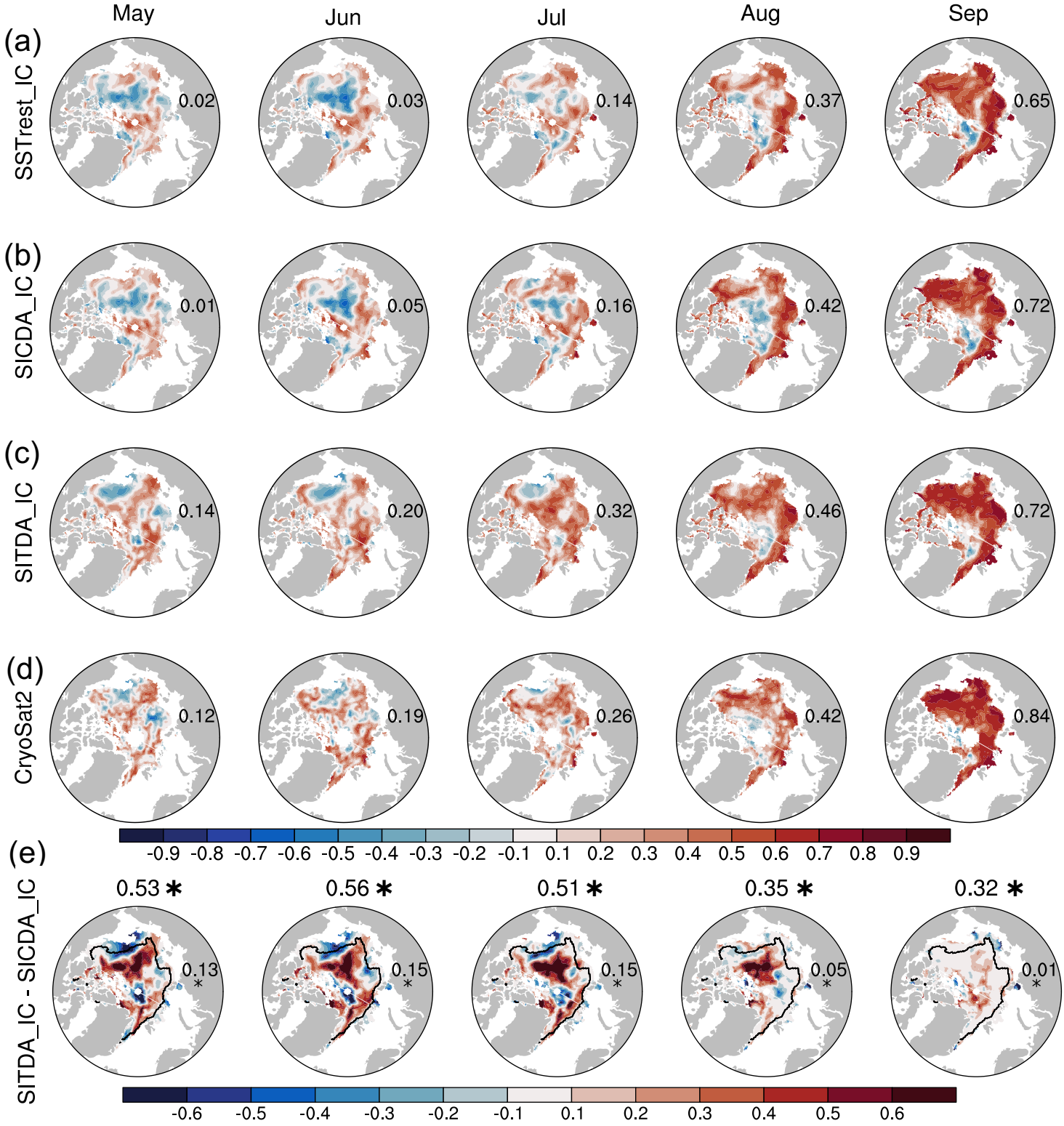
SIV correlation with observed September SIC
May
Jun
Jul
Aug
Sep
(a)
SSTrest_IC
0.02
0.03
0.14
0.37
0.65
(b)
SICDA_IC
0.01
0.05
0.16
0.42
0.72
(c)
SITDA_IC
0.14
0.20
0.32
0.46
0.72
(d)
CryoSat2
0.12
0.19
0.26
0.42
0.84
-0.9 -0.8 -0.7 -0.6 -0.5 -0.4 -0.3 -0.2 -0.1 0.1 0.2 0.3 0.4 0.5 0.6 0.7 0.8 0.9
(e)
SITDA_IC - SICDA_IC
0.53 *
0.56 *
0.51 *
0.35 *
0.32 *
0.13 *
0.15 *
0.15 *
0.05 *
0.01 *
-0.6 -0.5 -0.4 -0.3 -0.2 -0.1 0.1 0.2 0.3 0.4 0.5 0.6